



GEORG-AUGUST-UNIVERSITÄT
GÖTTINGEN

Fakultät für
Physik

Bachelor's Thesis

Hier steht das Thema der Arbeit in deutsch

Here comes the title of the thesis in english

prepared by

Timo Janßen

from Westerstede

at the Institut für heftige Physik

Thesis period: 1. Januar 2000 until 1. Januar 2000

Supervisor: Dr. X

First referee: Prof. Dr. X

Second referee: Prof. Dr. Newton

Kurzfassung

<insert your name>

<insert title>

Schlagwörter: <insert key words>

Abstract

<insert your name>

<insert title (english)>

Key words: <insert key words>

Inhaltsverzeichnis

1 Einleitung	1
2 Grundlagen	3
2.1 Next-to-leading order calculations	3
2.2 Reweighting QCD calculations	6
2.3 Interpolation grids	8
2.4 The considered process: Higgs production through gluon fusion	10
2.5 Leptonic Higgs decay	13
3 Experimentelle Vorgehensweise	15
3.1 ???	15
4 Results	19
4.1 Grid validation	19
4.1.1 Interpolation accuracy	20
5 Diskussion	29
Anhang	37
Literatur	37
Liste der noch zu erledigenden Punkte	44

KAPITEL 1

Einleitung

KAPITEL 2

Grundlagen

2.1 Next-to-leading order calculations

...(need real and virtual, both separately divergent, need to regularize)

There are two general methods that are commonly used to take care of the infrared divergences in NLO calculations, namely the *slicing method* and the *subtraction method*. We can demonstrate both methods with a simple example similar to the depiction in [26]. Consider the integral

$$I = \lim_{\epsilon \rightarrow 0} \left(\int_0^1 \frac{dx}{x} x^\epsilon F(x) - \frac{1}{\epsilon} F(0) \right), \quad (2.1)$$

where $F(x)$ is an arbitrary function that depends on x . The first term contains a singularity at $x = 0$ and is divergent in the limit $\epsilon \rightarrow 0$. This divergence is canceled by the second term. The parameter ϵ can be compared to the parameter used in dimensional regularization. As a consequence of $F(x)$ being arbitrary complex, the integral can not be solved analytically. However, in this form it is also not well-suited for a numerical evalution because of the presence of ϵ in the integrand.

In the slicing method, one introduces a small parameter δ , which slices the integration region into two pieces, so that the integral can be written in the following

way:

$$\begin{aligned}
I &= \lim_{\epsilon \rightarrow 0} \left(\int_0^\delta \frac{dx}{x} x^\epsilon F(x) + \int_\delta^1 \frac{dx}{x} x^\epsilon F(x) - \frac{1}{\epsilon} F(0) \right) \\
&= \lim_{\epsilon \rightarrow 0} \left(F(0) \int_0^\delta \frac{dx}{x} x^\epsilon - \frac{1}{\epsilon} F(0) \right) + \int_\delta^1 \frac{dx}{x} F(x) + \mathcal{O}(\delta) \\
&= F(0) \lim_{\epsilon \rightarrow 0} \frac{\delta^\epsilon - 1}{\epsilon} + \int_\delta^1 \frac{dx}{x} F(x) + \mathcal{O}(\delta) \\
&= F(0) \ln \delta + \int_\delta^1 \frac{dx}{x} F(x) + \mathcal{O}(\delta). \tag{2.2}
\end{aligned}$$

Therefore, the dependence on ϵ has vanished completely and the remaining integral can be computed numerically. The terms $\mathcal{O}(\delta)$ are neglectable if δ is small. In an actual calculation, one would have to check that the result does not depend on the choice of δ .

The subtraction method does not involve any approximations. Instead, one rewrites the integral in the form

$$\begin{aligned}
I &= \lim_{\epsilon \rightarrow 0} \left(\int_0^1 \frac{dx}{x} x^\epsilon [F(x) - F(0)] + F(0) \int_0^1 \frac{dx}{x} x^\epsilon - \frac{1}{\epsilon} F(0) \right) \\
&= \int_0^1 \frac{dx}{x} [F(x) - F(0)], \tag{2.3}
\end{aligned}$$

which automatically leads to a form that can be evaluated by a numerical integration algorithm. We can take a look at how this method works in a somewhat more realistic calculation. Consider the expression for the expectation value of an infrared-safe observable O at NLO accuracy, consisting of a Born (B), a virtual (V) und a real (R) term:

$$\langle O \rangle = \lim_{\epsilon \rightarrow 0} \int_0^1 dx x^{-2\epsilon} O(x) \left[\left(\frac{d\sigma}{dx} \right)_B + \left(\frac{d\sigma}{dx} \right)_V + \left(\frac{d\sigma}{dx} \right)_R \right]. \tag{2.4}$$

We assume that the cross sections can be written as

$$\left(\frac{d\sigma}{dx}\right)_B = B\delta(x), \quad (2.5)$$

$$\left(\frac{d\sigma}{dx}\right)_V = a \left(\frac{B}{2\epsilon} + V\right) \delta(x), \quad (2.6)$$

$$\left(\frac{d\sigma}{dx}\right)_R = a \frac{R(x)}{x} \quad (2.7)$$

where B and V are constant factors and $\lim_{x \rightarrow 0} R(x) = B$. a denotes the coupling constant. This model has been adapted from [20]. Obviously, both the real and the virtual part are divergent in the limit $\epsilon \rightarrow 0$. Using the subtraction method analogous to the case above, we can rewrite the real contribution to obtain

$$\begin{aligned} \langle O \rangle_R &= a \lim_{\epsilon \rightarrow 0} \int_0^1 \frac{dx}{x^{1+2\epsilon}} O(x) R(x) \\ &= a BO(0) \lim_{\epsilon \rightarrow 0} \int_0^1 \frac{dx}{x^{1+2\epsilon}} + a \int_0^1 \frac{dx}{x} [O(x)R(x) - BO(0)] \\ &= -a BO(0) \lim_{\epsilon \rightarrow 0} \frac{1}{2\epsilon} + a \int_0^1 \frac{dx}{x} [O(x)R(x) - BO(0)]. \end{aligned} \quad (2.8)$$

By explicitly writing down the virtual part,

$$\langle o \rangle_V = a \lim_{\epsilon \rightarrow 0} \int_0^1 \frac{dx}{x^{2\epsilon}} O(x) \left(\frac{B}{2\epsilon} + V\right) \delta(x), \quad (2.9)$$

we see that the first term gets exactly cancelled by the first term on the right hand side of (2.8). Including the Born contribution we arrive at the expression

$$\langle O \rangle = BO(0) + a \left\{ VO(0) + \int_0^1 \frac{dx}{x} [O(x)R(x) - BO(0)] \right\}, \quad (2.10)$$

which now only consists of finite terms.

The subtraction method can be generalized to arbitrary hadronic cross sections, provided that the definition of the observables allows the cancellation of the diver-

gences. In simplified terms, it always leads to an expression of the form

$$\sigma_{pp \rightarrow X}^{\text{NLO}} = \int d\hat{\sigma}^B + \int d\hat{\sigma}^V + \int d\hat{\sigma}^I + \int d\hat{\sigma}^{RS} \quad (2.11)$$

consisting of a Born (B), a virtual (V), an integrated subtraction (I) and a real subtracted (RS) term. All of these terms are separately finite.

2.2 Reweighting QCD calculations

Often it is needed to vary the parameters in QCD calculations, for example the scale variables and PDFs to estimate the uncertainty. When the number of variations becomes large, it is not practical to rerun the whole event generation for each calculation as the time and resource consumption become too high. Instead it is possible to reuse information from previously generated events and combine them with the new parameters. For a leading order calculation, this is straightforward: Consider the leading order parton model cross section for producing an arbitrary final state X:

$$\sigma_{pp \rightarrow X} = \sum_{i,j} \int dx_1 dx_2 \int d\Phi_n \left(\frac{\alpha_s(\mu_R^2)}{2\pi} \right)^{p_{\text{LO}}} f_i(x_1, \mu_F^2) f_j(x_2, \mu_F^2) d\hat{\sigma}_{ij \rightarrow X}. \quad (2.12)$$

The squared matrix element for the parton-level subprocess $2 \rightarrow n$ is denoted by $d\hat{\sigma}_{ij \rightarrow X}$, differential in the phase space $d\Phi_n$. We can group subprocesses s with the same parton-level cross section into a cumulated parton density $F_s(x_1, x_2, \mu_F^2)$ and write

$$\sigma_{pp \rightarrow X} = \int dx_1 dx_2 \int d\Phi_n \left(\frac{\alpha_s(\mu_R^2)}{2\pi} \right)^{p_{\text{LO}}} F_s(x_1, x_2, \mu_F^2) d\hat{\sigma}_{ij \rightarrow X}. \quad (2.13)$$

Rewriting this in a form that can be computed by a Monte Carlo algorithm on a per-event basis, we arrive at

$$\sigma_{pp \rightarrow X} = \sum_{e=1}^{N_{\text{evt}}} \left(\frac{\alpha_s(\mu_R^2)}{2\pi} \right)^{p_{\text{LO}}} w_e(k_e) F_{s_e}(x_1, x_2, \mu_F^2). \quad (2.14)$$

The event weight $w_e(k_e)$ is given by

$$w_e(k_e) = \Pi_{\text{ps}}(k_e) \Theta(k_e - k_{\text{cuts}}) d\hat{\sigma}_e \quad (2.15)$$

and represents the subprocess cross section $d\hat{\sigma}_e$ with respect to the phase space weight $\Pi_{\text{ps}}(k_e)$ and the kinematic cuts. The kinematic parameters for each event are combined in

$$k_e = \{p_1, \dots, p_n, x_1, x_2\}, \quad (2.16)$$

where the p_i denote the involved partons.

Provided that all event weights have been stored, using a different PDF is as simple as multiplying each weight with the new PDF $F_{s_e}^{\text{new}}(x_1, x_2, \mu_F^2)$. The value of α_s can be changed similarly. To vary the scales, only α_s and F_{s_e} have to be reevaluated as the weights themselves do not depend on the scales.

At NLO the reweighting becomes more involved. The event weights now depend explicitly on the scales and due to the appearance of divergences in the calculation of the parton-level cross sections, a method for cancelling these divergences has to be used. In the following, we will examine the method used by **MCgrid** to reweight NLO calculations. It expects, that the events are generated using the Catani-Seymour dipole subtraction method [8], which is a general algorithm for the automatic calculation of arbitrary jet cross sections at NLO. It is based on the subtraction method introduced in §2.1.

As we have seen, the subtraction method splits the calculation into four parts: The Born (B), virtual (V), integrated subtraction (I) and real subtraction (RS) part. All of these have to be handled differently. How this is done in detail can be seen in the original **MCgrid** paper [13]. The important result is, that if we treat the different

contributions as single events, the NLO result can be written in a form similar to the LO expression (2.14):

$$\sigma_{pp \rightarrow X}^{\text{NLO}} = \sum_{e=1}^{N_{\text{evt}}} \left(\frac{\alpha_s(\mu_R^2)}{2\pi} \right)^{p_e} w_e(k_e) F_{s_e}(x_1, x_2, \mu_F^2), \quad (2.17)$$

where p_e is the order in α_s of the respective event, i.e. $p_e = p_{\text{LO}}$ for B events and $p_e = p_{\text{LO}} + 1$ for I, V and RS events. This allows for simple *a posteriori* parameter variation analogous to the LO case.

2.3 Interpolation grids

Despite the advantage towards regenerating all events for the variation of a single parameter, the reweighting approach is still not a satisfying solution for many use cases. The whole event record has to be stored, which can easily reach many gigabytes in high statistics computations. The storing and reprocessing of the events may be a challenge by itself and is not convenient if more than a few parameter variations have to be performed. One therefore wishes to somehow decrease the resource requirements without losing a significant amount of accuracy. In the ideal case, it should be mostly independent on the statistics. A possible solution is the use of interpolating grids to represent the PDFs and event weights. Then only a uniquely defined number of values has to be saved, while values in-between the grid points are generated by interpolating functions. Such a method has been implemented by the **APPLGRID** [7] and **fastNLO** [25, 29] projects.

The PDF $f(x, Q^2)$ depends on the momentum fraction x and the momentum transfer Q^2 . It can be approximated as a sum over discrete grid points using interpolation functions I of order N :

$$f(x, Q^2) = \sum_{i=0}^{N_x} \sum_{j=0}^{N_Q} f(x_i, Q_j^2) I_i^{(N_x)}(x) I_j^{(N_Q)}(Q^2). \quad (2.18)$$

Transferred to the subprocess PDF $F_s(x_1, x_2, Q^2)$ defined above, the interpolation

takes the form

$$F_s(x_1, x_2, Q^2) = \sum_{i,j=0}^{N_x} \sum_{k=0}^{N_Q} F_s(x_i, x_j, Q_k^2) I_i^{(N_x)}(x_1) I_j^{(N_x)}(x_2) I_k^{(N_Q)}(Q^2). \quad (2.19)$$

Consequently, we can write (2.17) as

$$\begin{aligned} \sigma_{pp \rightarrow X}^{\text{NLO}} &= \sum_{e=1}^{N_{\text{evt}}} \sum_{i,j=0}^{N_x} \sum_{k=0}^{N_Q} \left(\frac{\alpha_s(Q_k^2)}{2\pi} \right)^{p_e} w_e(k_e) F_{s_e}(x_i, x_j, Q_k^2) \\ &\quad \cdot I_i^{(N_x)}(x_1) I_j^{(N_x)}(x_2) I_k^{(N_Q)}(Q^2) \\ &= \sum_p \sum_{s=0}^{N_{\text{sub}}} \sum_{i,j=0}^{N_x} \sum_{k=0}^{N_Q} \left(\frac{\alpha_s(Q_k^2)}{2\pi} \right)^p W_{i,j,k}^{(p),(s)}(k_e) F_s(x_i, x_j, Q_k^2), \end{aligned} \quad (2.20)$$

where p is the perturbative order, N_{sub} is the number of different subprocesses and the interpolated weights $W_{i,j,k}^{(p),(s)}(k_e)$ are processed as a sum over the events:

$$W_{i,j,k}^{(p),(s)} = \sum_{e=1}^{N_{\text{evt}}} \delta_{p,p_e} \delta_{s,s_e} I_{i,j,k}^{(N_x)(N_Q)}(k_e) w_e(k_e) I_i^{(N_x)}(x_1) I_j^{(N_x)}(x_2) I_k^{(N_Q)}(Q^2). \quad (2.21)$$

Now the sum over the events is completely absorbed into the definition of the interpolated weights. These can be calculated in a single run of the event generator and be stored efficiently. The calculation of the cross section has become a simple sum over the grid points and thus is much faster for a large number of events. The approach can easily be extended to histogrammed data like differential cross sections by defining the observable bins and computing one weight $W_{i,j,k}^{(p),(s),(b)}$ for each bin b . However, unlike the full event record, the weight grid is restricted to the observable it was constructed for and cannot be used to calculate any other values.

While the variation of the PDF and α_s is still straightforward, scale variation is slightly more complicated because the weights themselves depend on the scale choices. Nevertheless, it is possible to vary the scales without too much effort, using DGLAP evolution. The precise procedure is explained in [7].

2.4 The considered process: Higgs production through gluon fusion

In this thesis, the considered process will be the production of a Higgs boson through gluon fusion. Although there are other possible production mechanisms in the Standard Model, this is the main process at the LHC, with an expected cross section of $\approx 50 \text{ pb}$ at a center-of-mass energy of $\sqrt{s} = 14 \text{ TeV}$ and a Higgs mass of 125 GeV [15]. It proceeds through a triangular loop of heavy quarks (mainly top quarks as the Higgs coupling scales with the quark mass) as is shown in Figure 2.1.

In the narrow-width approximation, the leading order cross section is given by [21]

$$\sigma_{\text{LO}}(pp \rightarrow H) = \sigma_0^H \tau_H \frac{d\mathcal{L}^{gg}}{d\tau_H}, \quad (2.22)$$

where $\tau_H = M_H^2/s$ is the Drell-Yan variable and $d\mathcal{L}^{gg}/d\tau_H$ is the gluon luminosity. The partonic cross section σ_0^H can be written as

$$\sigma_0^H = \frac{G_F \alpha_s^2(\mu_R^2)}{288\sqrt{2}\pi} \left| \sum_q \frac{3}{2\tau_q} \left[1 + \left(1 - \frac{1}{\tau_q} \right) f(\tau_q) \right] \right|^2, \quad (2.23)$$

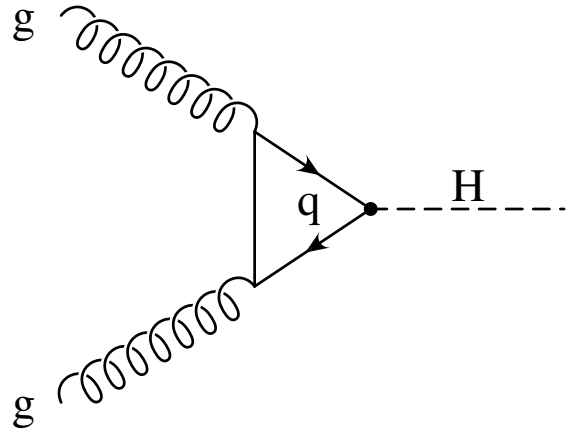


Abbildung 2.1: Higgs production through gluon fusion.

with the form factor

$$f(\tau_q) = \begin{cases} \arcsin^2(\sqrt{\tau_q}), & \tau_q < 1, \\ -\frac{1}{4} \left[\ln \frac{1+\sqrt{1-\tau_q^{-1}}}{1-\sqrt{1-\tau_q^{-1}}} - i\pi \right]^2, & \tau_q > 1, \end{cases} \quad (2.24)$$

where G_F denotes the Fermi coupling constant and $\tau_q = m_H^2/4m_q^2$. The gluon luminosity takes the form

$$\frac{d\mathcal{L}^{gg}}{d\tau_H} = \int_0^1 dx_1 dx_2 g(x_1, \mu_F^2) g(x_2, \mu_F^2) \delta(x_1 x_2 - \tau_q) \quad (2.25)$$

with $g(x, \mu_F^2)$ denoting the gluon PDF.

The QCD corrections are composed of virtual corrections to the vertices and propagators, real gluon radiation in the initial state and the contributions of the subprocesses $gq \rightarrow Hq$ and $q\bar{q} \rightarrow Hg$. Exemplary diagrams for the corrections are shown in Figure 2.2.

The NLO QCD corrections to the cross section have been calculated in [22]. They increase the cross section by a factor of 1,5 to 1,7. In the limit where the top quark has infinite mass, $m_t \rightarrow \infty$, the form factor takes the value $\frac{4}{3}$. This allows for an analytical expression for the corrections [17], which is very well suited for numerical calculations. It can be considered as an extension of the Standard Model, where the Higgs boson couples directly to gluons (effective Higgs coupling). In many cases, this is a rather good approximation [18].

The NNLO corrections have been calculated in [2, 23].

A fully differential NNLO calculation exists for $H + 0 - \text{jet}$ production [3, 9] and substantial progress has been achieved towards an NNLO calculation of the $1 - \text{jet}$ cross section [11]. The fully differential NLO cross section is available for $H + 1 - \text{jet}$ [19, 28], $H + 2 - \text{jets}$ [6, 14] and $H + 3 - \text{jets}$ [12].

The effective Lagrangian for Higgs gluon interaction can be written as [2]

$$\mathcal{L}_{\text{eff}}^{ggH} = -\frac{1}{4v} C_1 G_{\mu\nu}^a G^{a\mu\nu} H, \quad (2.26)$$

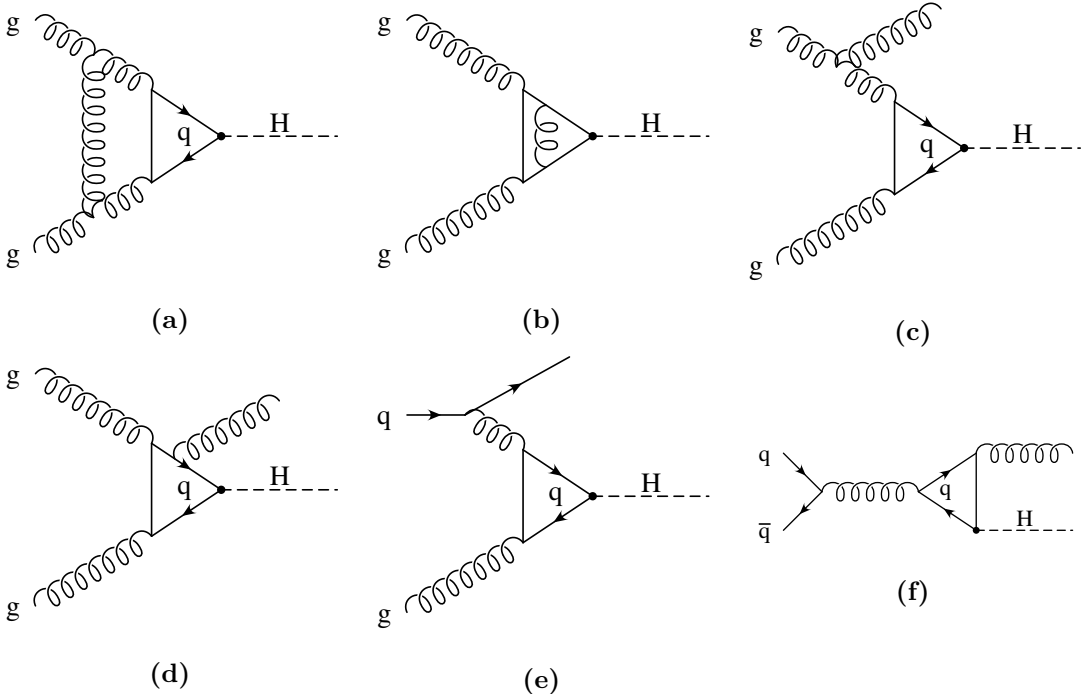


Abbildung 2.2: Example diagrams illustrating the QCD corrections to the process $pp \rightarrow H$: (a), (b) virtual corrections; (c), (d) real emission of a gluon; (e) $gq \rightarrow Hq$; (f) $q\bar{q} \rightarrow Hg$.

where v is the Higgs vacuum expectation value, $G_{\mu\nu}^a$ is the gluon field strength tensor and H is the Higgs field. The coefficient C_1 , in the $\overline{\text{MS}}$ scheme, is given by

$$C_1 = \frac{-1}{3\pi} \left\{ 1 + \frac{11\alpha_s}{4\pi} + \left(\frac{\alpha_s}{\pi} \right)^2 \left[\frac{2777}{288} + \frac{19}{16} \log \left(\frac{\mu^2}{m_t^2} \right) + n_f \left(-\frac{67}{96} + \frac{1}{3} \log \left(\frac{\mu^2}{m_t^2} \right) \right) \right] + \mathcal{O}(\alpha_s^3) \right\}, \quad (2.27)$$

where the number of active flavors should be set to $n_f = 5$. According to [2], at LO this approximation is accurate within 5 % for $m_H \approx 150 \text{ GeV}$ (which is close to the measured value $m_H \approx 126 \text{ GeV}$) and improves at NLO.

2.5 Leptonic Higgs decay

There are several possible decay channels for the Higgs boson. One has to keep in mind that the Higgs coupling is proportional to the particle masses, so that it will decay into the heaviest possible particles. Assuming a Higgs mass of $m_H = 126 \text{ GeV}$, the most relevant decay products are $q\bar{q}$ (where q denotes a bottom or charm quark), WW , ZZ , $Z\gamma$, $\gamma\gamma$, gg and $\tau^+\tau^-$ [16]. The decay into photons or gluons is only possible through intermediate loops.

The studies leading to the discovery of the Higgs boson at the LHC relied primarily on the decay modes $H \rightarrow \gamma\gamma$, $H \rightarrow ZZ$ and $H \rightarrow WW$.

...For the purpose of this thesis, we will consider the decay $H \rightarrow \tau^+\tau^-$, which has a branching ratio of approximately 6 % [24]. ...There have been searches for $H \rightarrow \tau\tau$ events in the LHC data and both ATLAS [1] and CMS [10] have published evidences for this type of decay.

KAPITEL 3

Experimentelle Vorgehensweise

3.1 ???

APPLGRID and `fastNLO` do not use the momentum fraction x and the factorization scale Q^2 directly in their grids. Instead they provide transformations that are supposed to achieve better coverage of the values. In the following we will concentrate on the x distribution, which is more crucial to the number of grid points needed. The functions provided by APPLGRID are:

$$f_0(x) = \log\left(\frac{1}{x} - 1\right) \quad (3.1)$$

$$f_1(x) = -\log(x) \quad (3.2)$$

$$f_2(x) = \sqrt{-\log(x)} \quad (3.3)$$

$$f_3(x) = -\log(x) + 5 \cdot (1 - x). \quad (3.4)$$

`fastNLO` only provides the functions $f_1(x)$ and $f_2(x)$. To be used in a grid, the functions are divided into equal-sized bins. In order to avoid empty bins, the limit values are determined in a separate „phasespace run“ before the actual fill run.

The functions (normalized to the domain $[0, 1]$ for comparability) are shown in Figure 3.1. All transformations increase the point density in the low x region, where most events should fall into. Compared against f_0 , the other functions also accomplish a higher point density in the high x region. Some observables in specific processes might benefit from this.

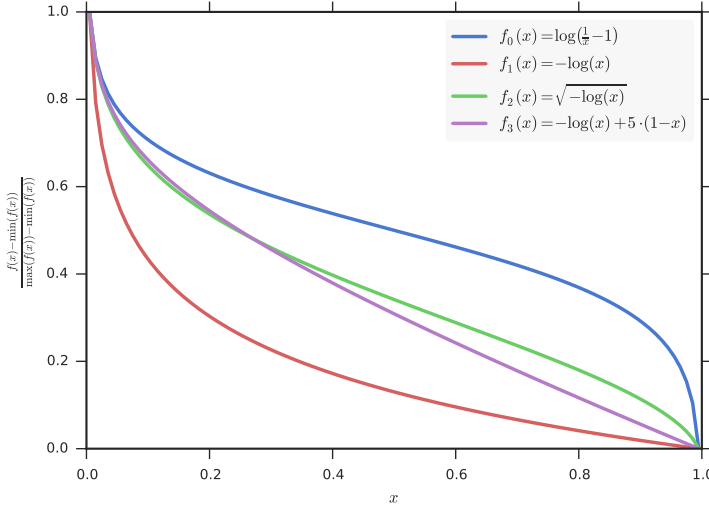


Abbildung 3.1: The transformations applied to the x distribution, normalized to the range $[0, 1]$.

We can look at the actual x distribution in the process considered in this thesis. In Figure 3.2 it is plotted for one of the gluons involved in the process $gg \rightarrow H + j$ at leading order for a center-of-mass energy of $\sqrt{s} = 13$ TeV. For comparison, the respective distribution for the functions f_1 to f_4 is also shown. In the bare distribution, the number of events per bin increases rapidly towards low x . It is obvious that the reproduction of the low x region is poor for this linear binning. We expect that for some $x > 0$ the number of events approaches zero, because there has to be at least enough momentum transfer to produce the Higgs boson and the jet. To see this with linear binning, one would need a huge amount of bins. In contrast, the transformations are able to project the low x peak to a higher number of bins than the naive linear binning. Additionally, they all approach zero for a finite value (note that high values of $f(x)$ correspond to low values of x). Due to the normalization, this happens at 1. For all transformed distributions, it should be possible to interpolate them with a reasonable number of sampling points. The function $f_1(x)$ looks most promising, as it allocates many bins for the peak region, which should be the most relevant for this process.

If we want to be more specific, we can extract the dependence of the observables

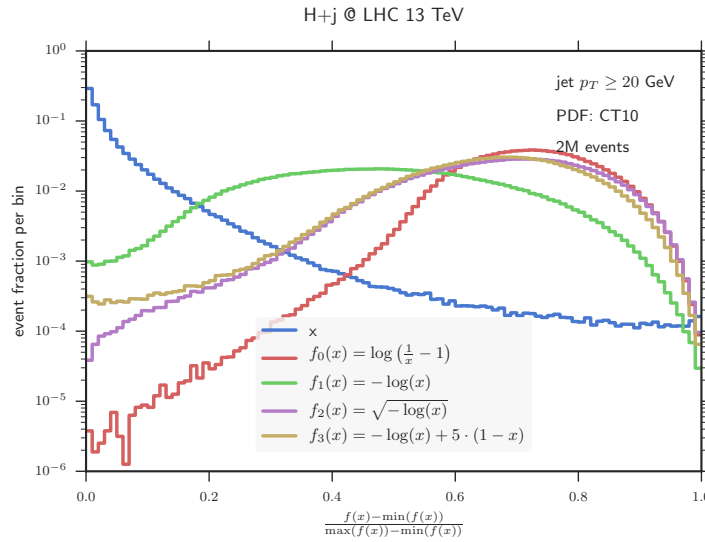


Abbildung 3.2: The event fraction per bin for the different transformations.

on x and $f(x)$, respectively, from the generated events. This is shown in Figure 3.3 for the transverse momentum p_\perp and in Figure 3.4 for the rapidity y of the Higgs boson. For both observables all considered functions are reasonable. Again, the function $f_1(x)$ seems to be best suited. Hence, it will be the transformation used in all following grid calculations.

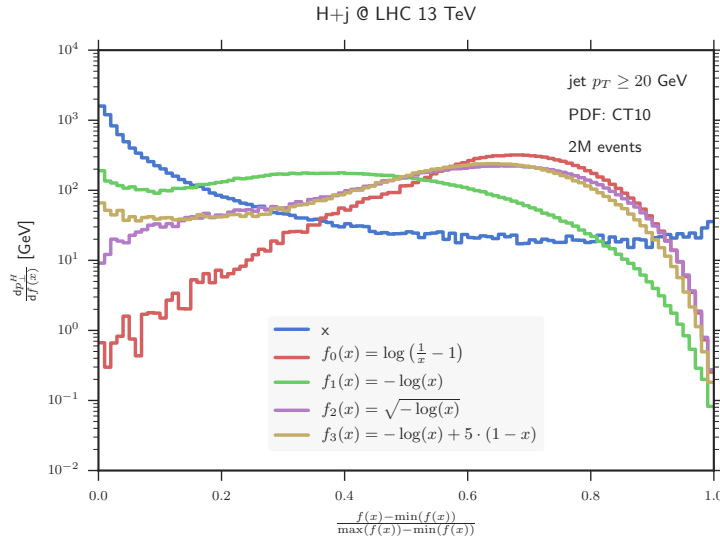


Abbildung 3.3: The transverse momentum p_\perp of the Higgs boson differential in the momentum fraction x of one of the gluons.

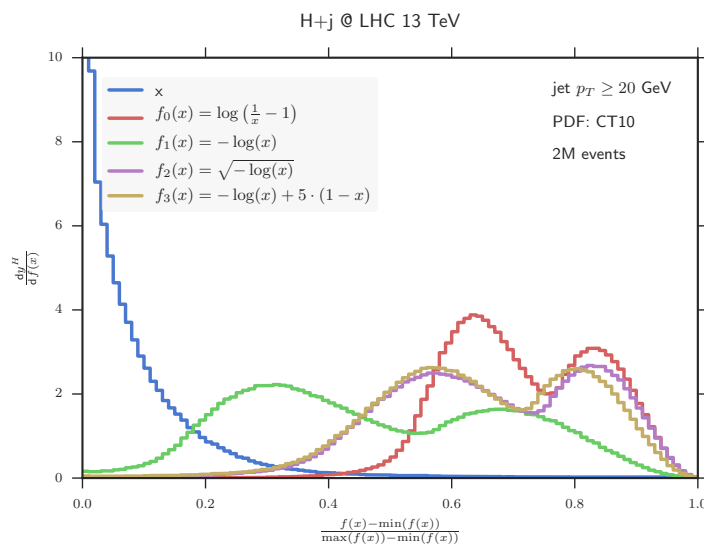


Abbildung 3.4: The rapidity y of the Higgs boson differential in the momentum fraction x of one of the gluons.

KAPITEL 4

Results

4.1 Grid validation

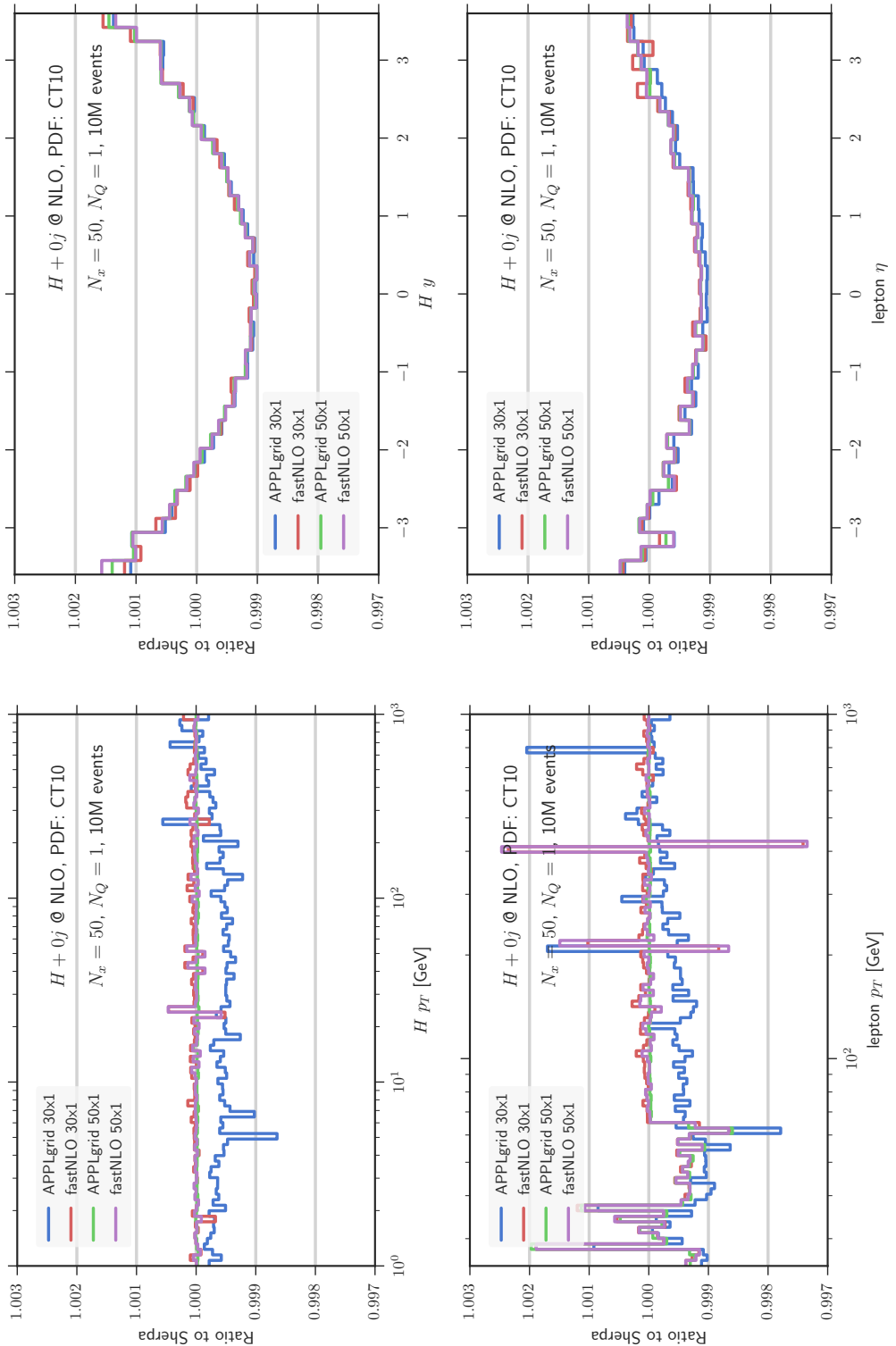
In the following we will validate the interpolation method used by `MCgrid` for the processes $pp \rightarrow H + (0, 1, 2)\text{jets}$ at the 13 TeV LHC, computed at NLO. Thereto, we generate reference distributions for different observables using the `SHERPA` event generator and compare them to the distributions obtained by convoluting a grid with the respective PDF. When possible, the results from `APPLGRID` and `fastNLO` are compared to each other. All grids are filled using the central value of the CT10 pdf set [27]. The examined observables are the transverse momenta p_\perp of the Higgs boson and the τ leptons, respectively, the rapidity y of the Higgs boson and the pseudorapidity η of the τ leptons. The projection of the observables into histogram bins is accomplished by the `Rivet` analysis system. Final state jets are extracted by the `FastJet` library [4] using the anti- k_t algorithm [5] with a radius parameter $R = 0.4$ and a p_\perp -cut of $p_\perp > 20\text{ GeV}$.

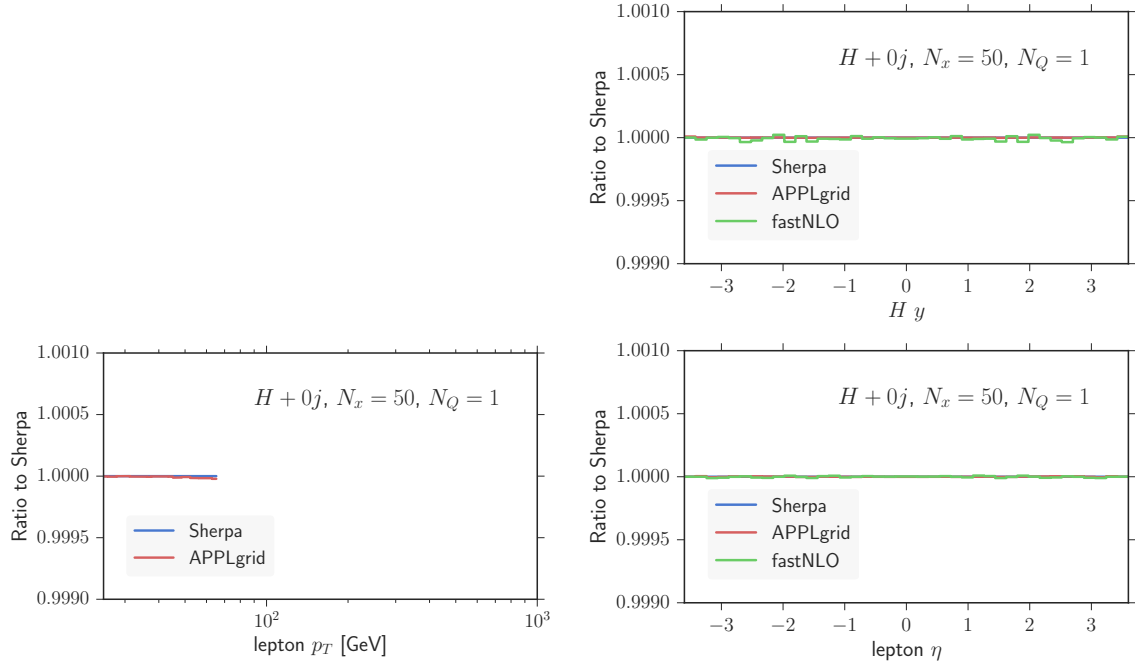
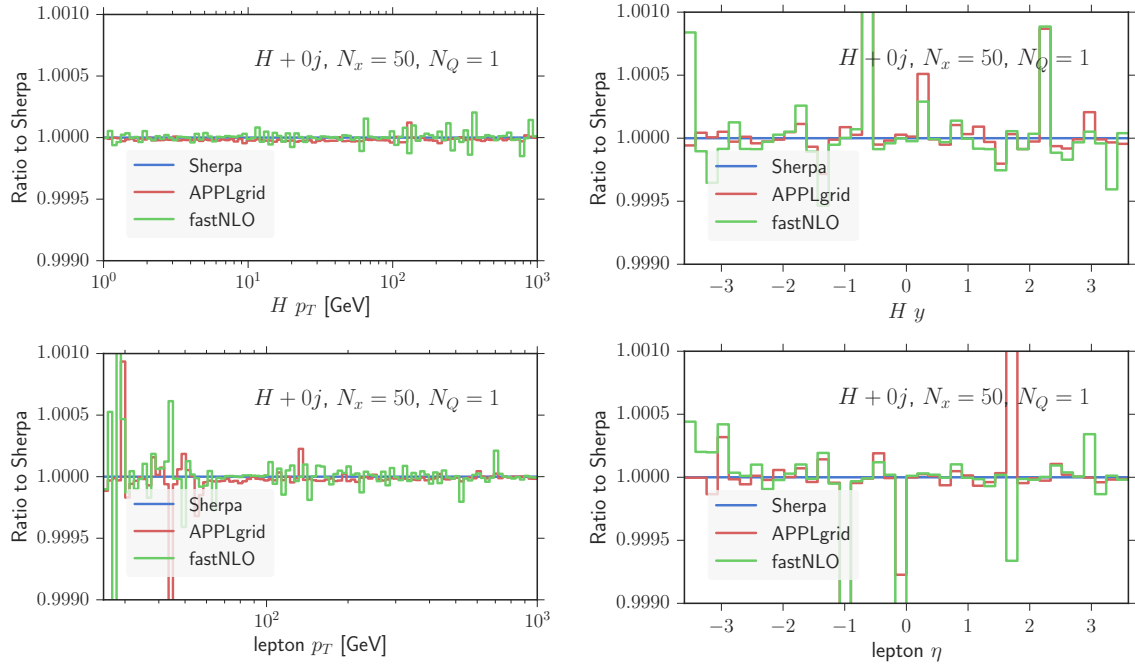
The first validity test will check whether the grids are able to reproduce the distributions when they are filled with the same events as the reference histograms, i.e. when no parameter variation is performed. This will also determine the interpolation accuracy. Subsequently, the cases where the scale factors and/or PDFs of the grids are changed *a posteriori* will be compared to reference distributions where these parameters have been set explicitly.

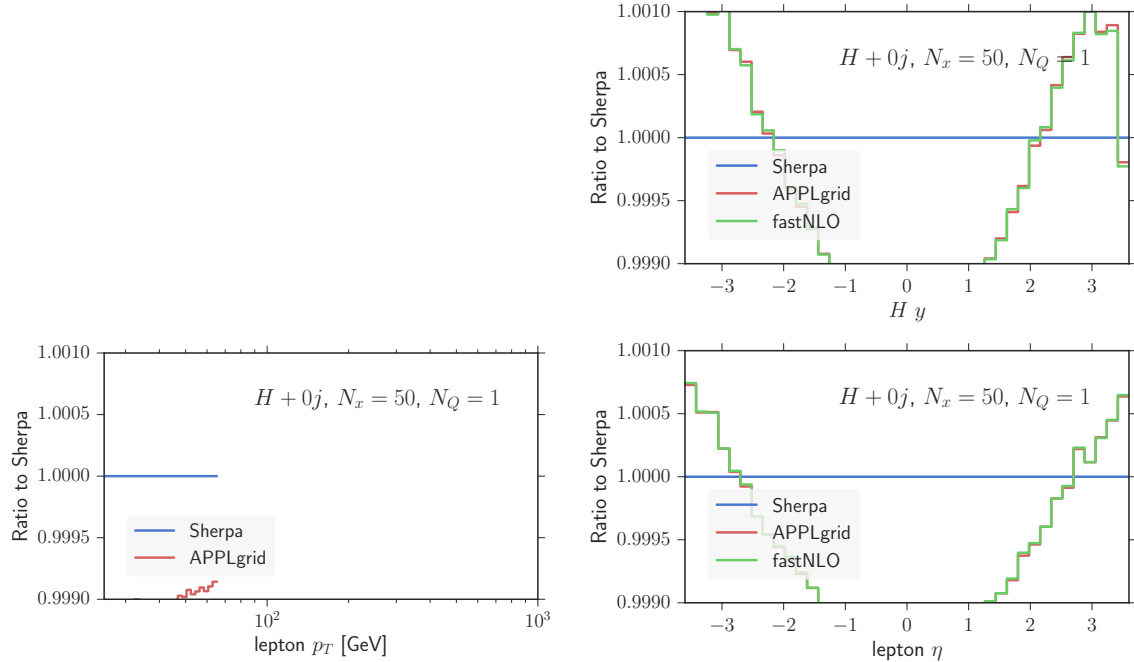
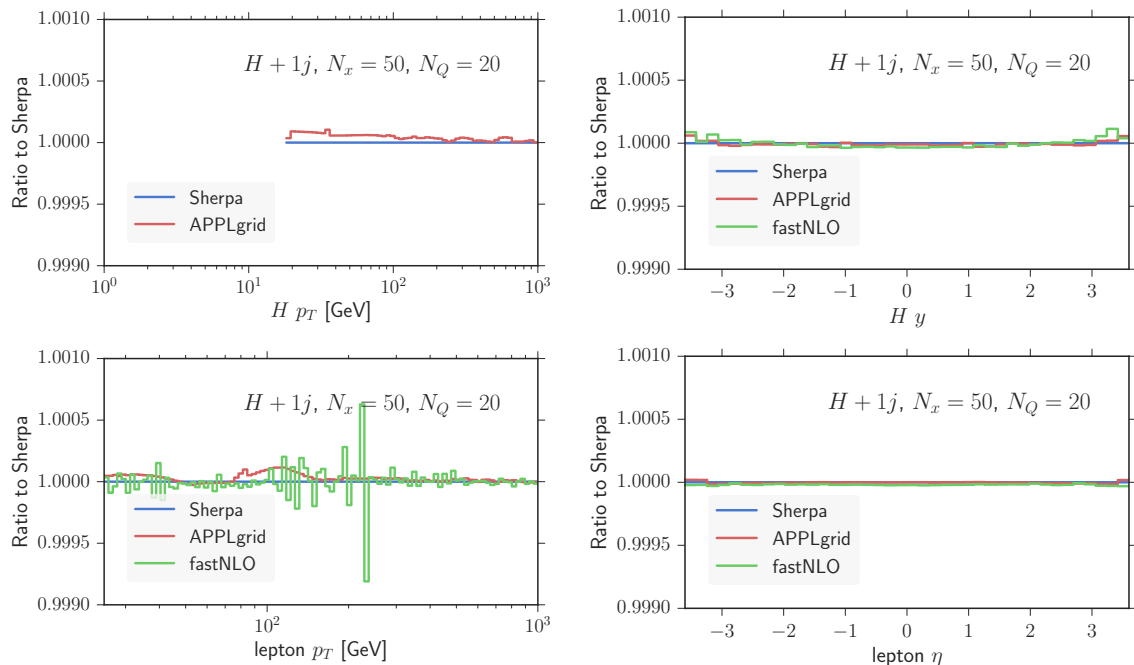
4.1.1 Interpolation accuracy

In this section we will prove, that the grids are able to reproduce the reference distributions up to the available interpolation accuracy. For each observable, two grids are produced: One high precision grid with 50 bins in x and 30 bins in Q^2 and one lower precision grid with 30 bins in x and **???** bins in Q^2 . In the 0-jet case, only one Q^2 bin is used, because the scale parameters are fixed to the Higgs boson mass so that Q^2 does not change. To achieve better comparability, APPLGRID is configured to use fourth order interpolation, which is the same as is hardcoded into the **fastNLO** library. A sample of 10 million events is used to fill the grids.

Abbildung 4.1 shows the ratio of the results obtained by convoluting the grids with the CT10 PDF to the reference distributions. In all cases, the reproduction accuracy is well below 1 % and for most of the bins it is even better than 0,1 %. The p_\perp distributions produced by APPLGRID are much more sensitive to the grid size than the ones produced by **fastNLO**. For the rapidity distributions, the differnce between the high and the low precision grid is negligible

**Abbildung 4.1:** $H + 0j$ NLO

**Abbildung 4.2:** H B**Abbildung 4.3:** H RS

**Abbildung 4.4:** H VI**Abbildung 4.5:** Hj B

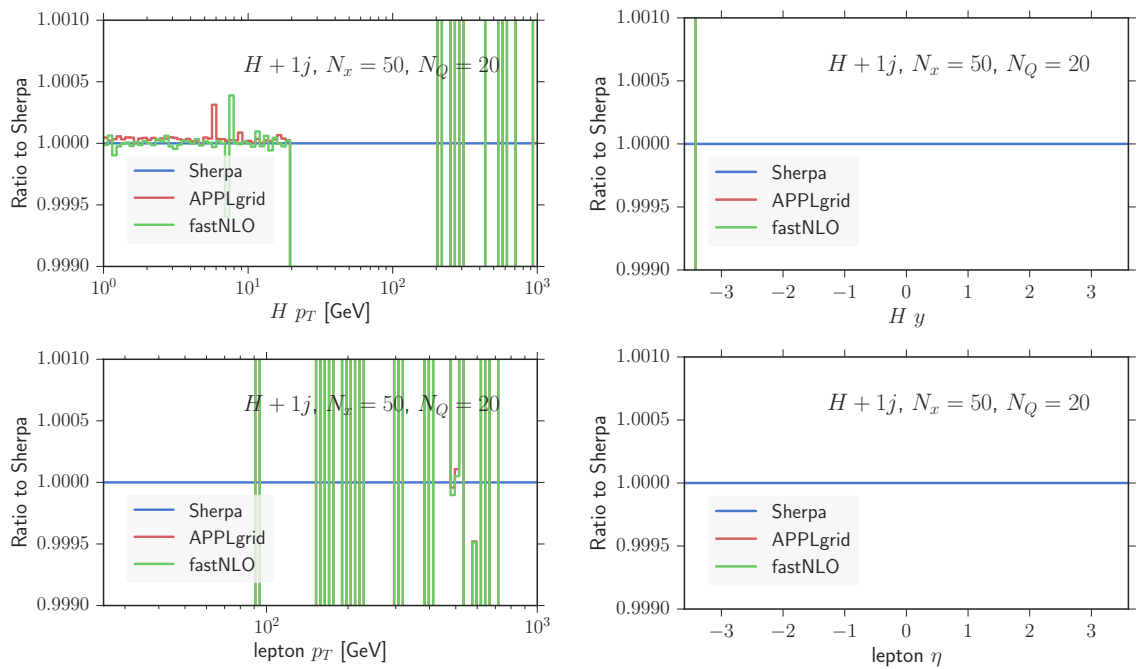


Abbildung 4.6: $H j$ RS

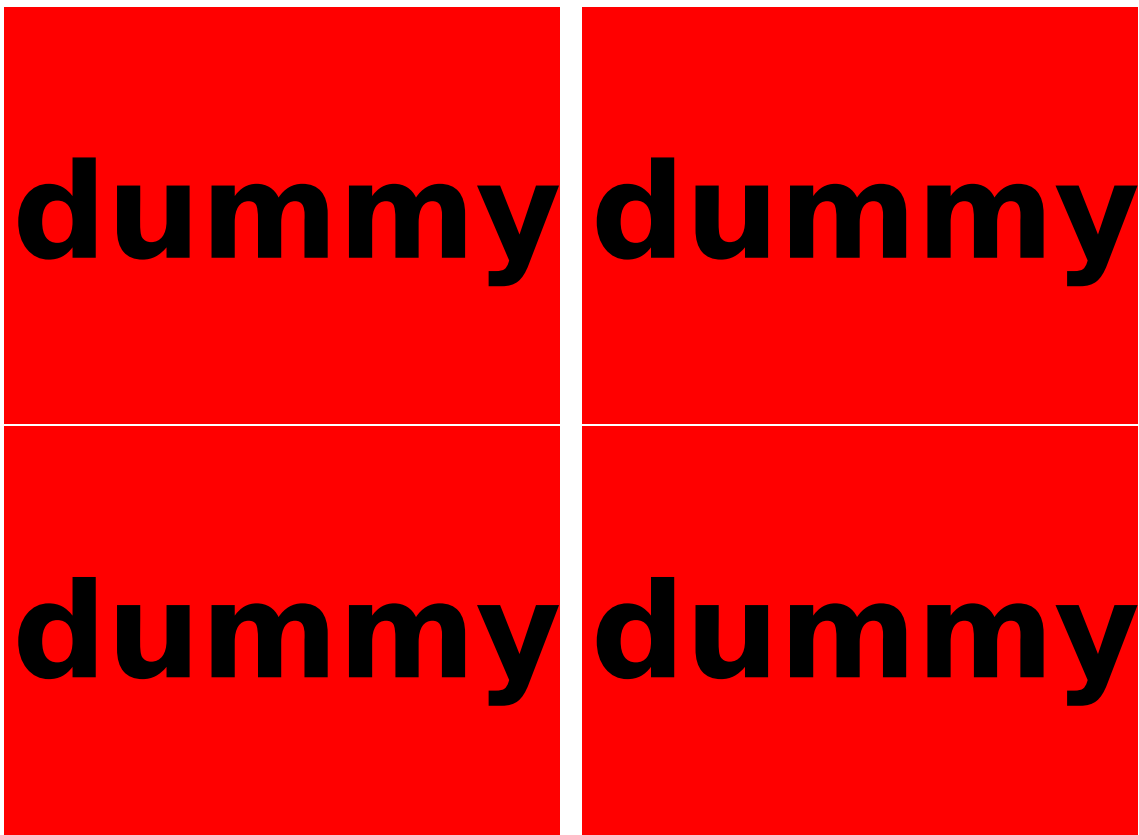


Abbildung 4.7: Hj VI

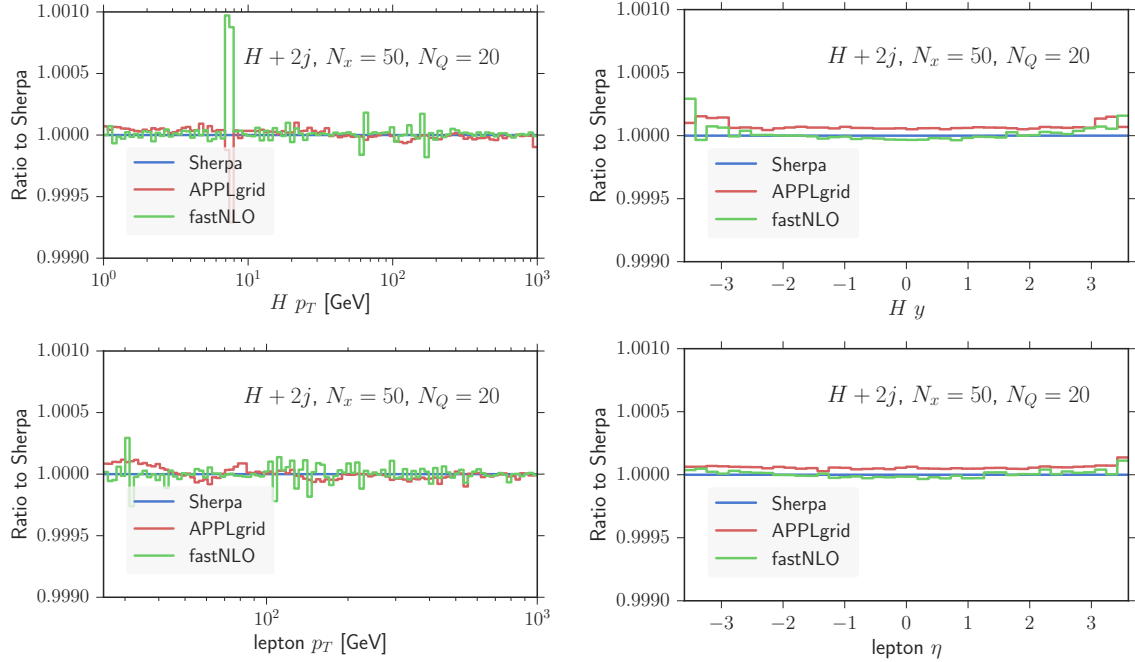


Abbildung 4.8: Hjj B

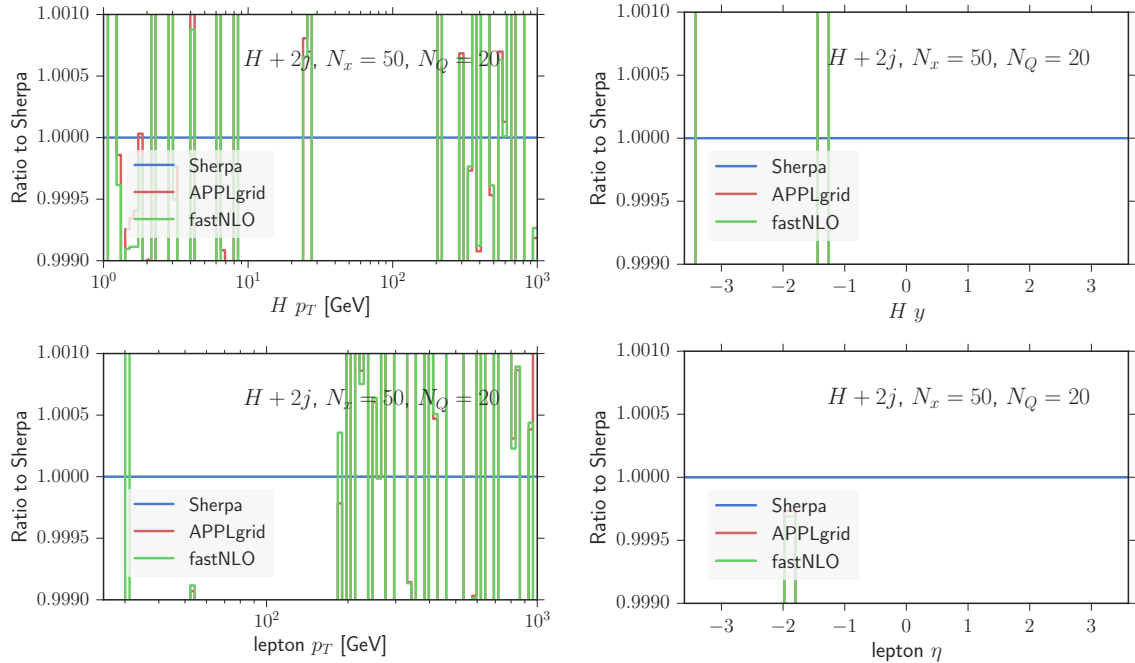


Abbildung 4.9: Hjj RS

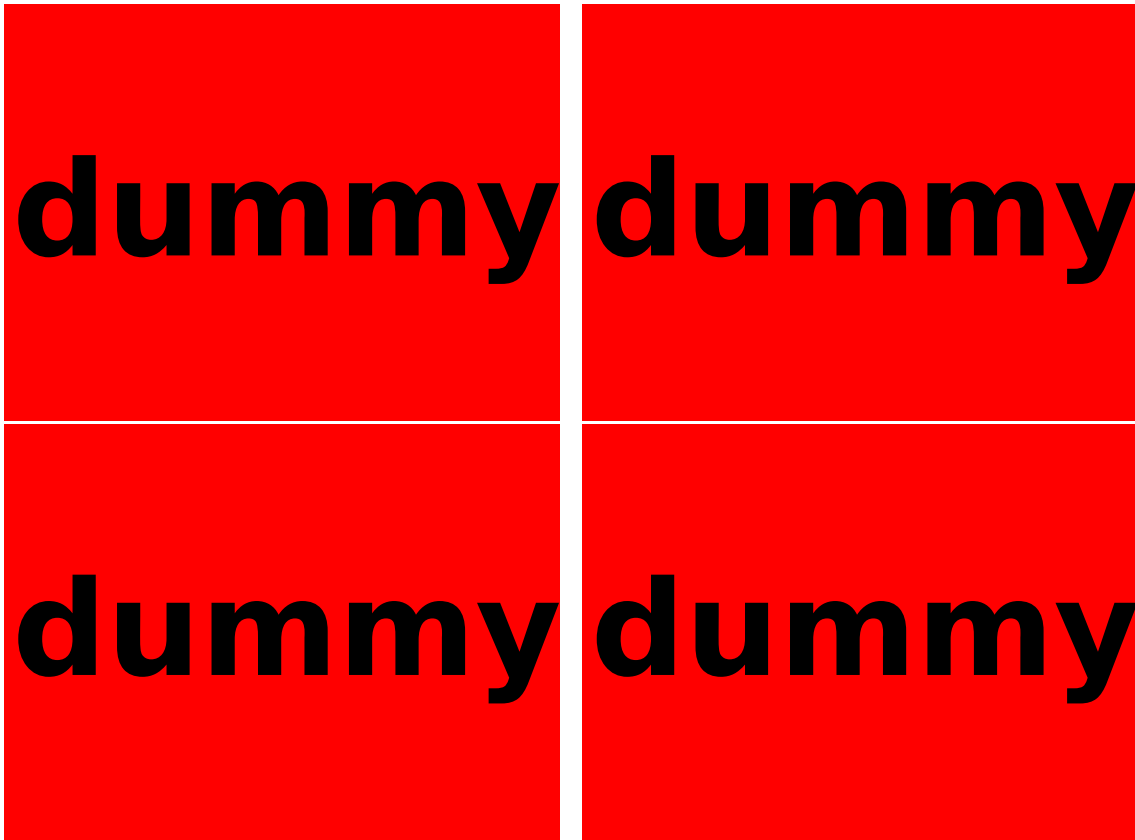


Abbildung 4.10: Hjj VI

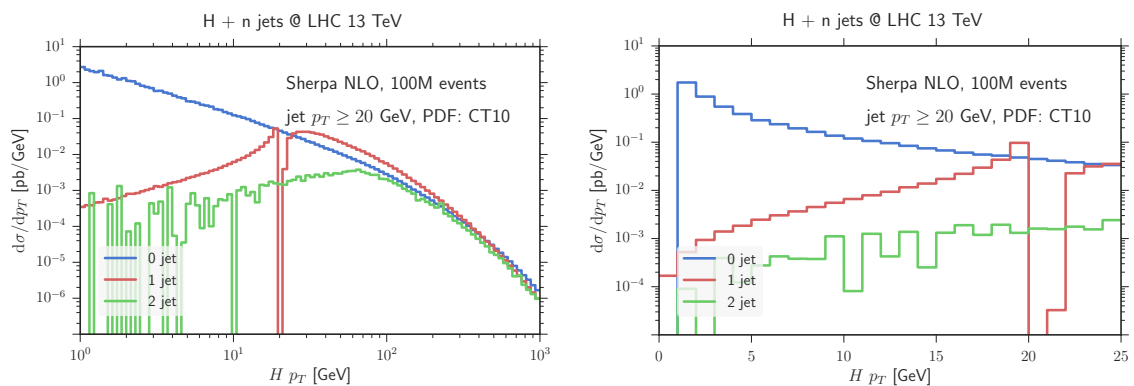


Abbildung 4.11: H pT NLO (0,1,2) jets

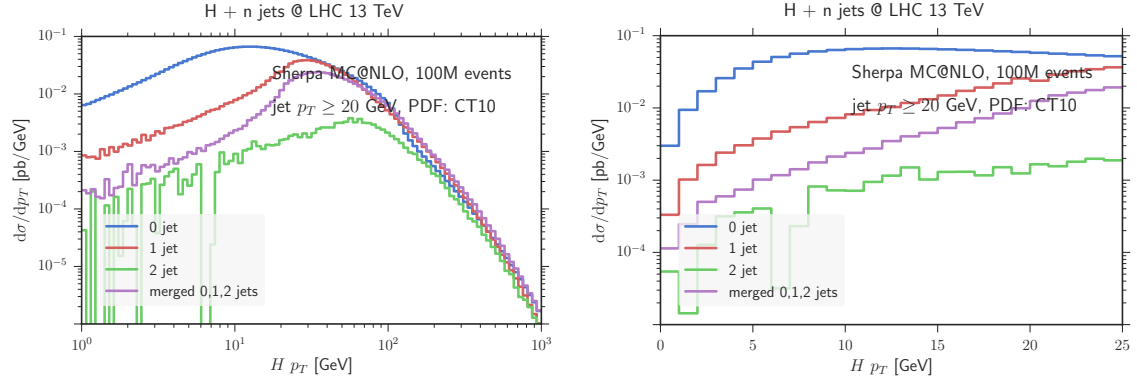
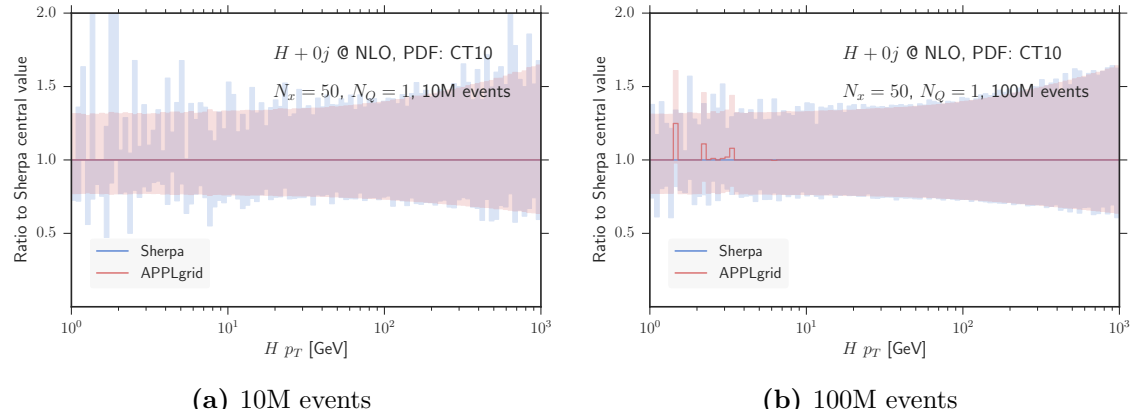


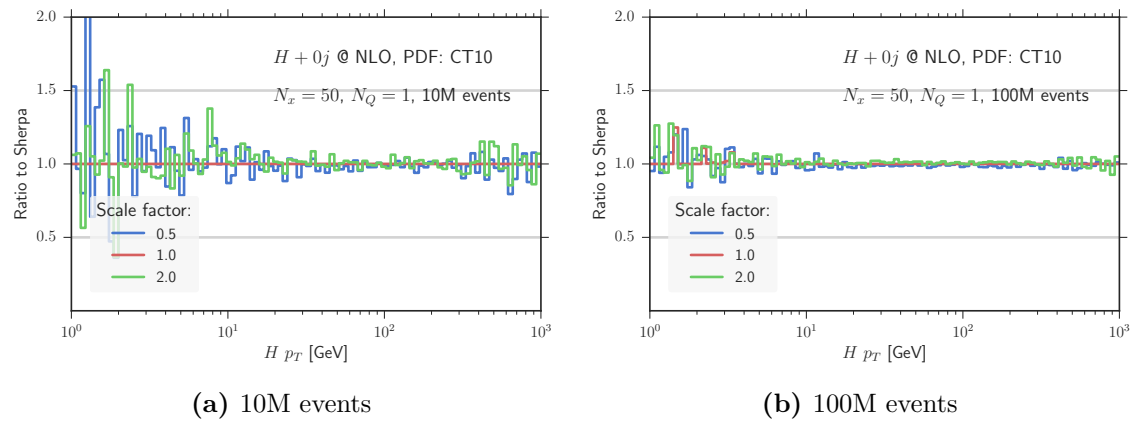
Abbildung 4.12: $H p_T$ MCatNLO (0,1,2) jets



(a) 10M events

(b) 100M events

Abbildung 4.13: Scale variations band



(a) 10M events

(b) 100M events

Abbildung 4.14: Scale variations ratio

KAPITEL 5

Diskussion

Abbildungsverzeichnis

2.1	Higgs production through gluon fusion.	10
2.2	Example diagrams illustrating the QCD corrections to the process $pp \rightarrow H$: (a), (b) virtual corrections; (c), (d) real emission of a gluon; (e) $gq \rightarrow Hq$; (f) $q\bar{q} \rightarrow Hg$	12
3.1	The transformations applied to the x distribution, normalized to the range $[0, 1]$	16
3.2	The event fraction per bin for the different transformations.	17
3.3	The transverse momentum p_{\perp} of the Higgs boson differential in the momentum fraction x of one of the gluons.	18
3.4	The rapidity y of the Higgs boson differential in the momentum fraction x of one of the gluons.	18
4.1	$H+0j$ NLO	21
4.2	H B	22
4.3	H RS	22
4.4	H VI	23
4.5	H_j B	23
4.6	H_j RS	24
4.7	H_j VI	25
4.8	H_{jj} B	26
4.9	H_{jj} RS	26
4.10	H_{jj} VI	27
4.11	H pT NLO (0,1,2) jets	27

4.12 H pT MCatNLO (0,1,2) jets	28
4.13 Scale variations band	28
4.14 Scale variations ratio	28

Tabellenverzeichnis

Listings

Literatur

1. AAD, GEORGES u. a.: „Evidence for the Higgs-boson Yukawa coupling to tau leptons with the ATLAS detector“. *JHEP* (2015), Bd. 1504: S. 117 (siehe S. 13).
2. ANASTASIOU, CHARALAMPOS und KIRILL MELNIKOV: „Higgs boson production at hadron colliders in NNLO QCD“. *Nucl.Phys.* (2002), Bd. B646: S. 220–256 (siehe S. 11, 12).
3. ANASTASIOU, CHARALAMPOS, KIRILL MELNIKOV und FRANK PETRIELLO: „Fully differential Higgs boson production and the di-photon signal through next-to-next-to-leading order“. *Nucl.Phys.* (2005), Bd. B724: S. 197–246 (siehe S. 11).
4. CACCIARI, MATTEO, GAVIN P. SALAM und GREGORY SOYEZ: „FastJet User Manual“. *Eur.Phys.J.* (2012), Bd. C72: S. 1896 (siehe S. 19).
5. CACCIARI, MATTEO, GAVIN P. SALAM und GREGORY SOYEZ: „The Anti-k(t) jet clustering algorithm“. *JHEP* (2008), Bd. 0804: S. 063 (siehe S. 19).
6. CAMPBELL, JOHN M., R. KEITH ELLIS und CIARAN WILLIAMS: „Hadronic production of a Higgs boson and two jets at next-to-leading order“. *Phys.Rev.* (2010), Bd. D81: S. 074023 (siehe S. 11).
7. CARLI, TANCREDI, DAN CLEMENTS, AMANDA COOPER-SARKAR, CLAIRE GWENLAN, GAVIN P. SALAM u. a.: „A posteriori inclusion of parton density functions in NLO QCD final-state calculations at hadron colliders: The APP-LGRID Project“. *Eur.Phys.J.* (2010), Bd. C66: S. 503–524 (siehe S. 8, 9).

8. CATANI, S. und M.H. SEYMOUR: „A General algorithm for calculating jet cross-sections in NLO QCD“. *Nucl.Phys.* (1997), Bd. B485: S. 291–419 (siehe S. 7).
9. CATANI, STEFANO und MASSIMILIANO GRAZZINI: „An NNLO subtraction formalism in hadron collisions and its application to Higgs boson production at the LHC“. *Phys.Rev.Lett.* (2007), Bd. 98: S. 222002 (siehe S. 11).
10. CHATRCHYAN, SERGUEI u. a.: „Evidence for the 125 GeV Higgs boson decaying to a pair of τ leptons“. *JHEP* (2014), Bd. 1405: S. 104 (siehe S. 13).
11. CHEN, X., T. GEHRMANN, E.W.N. GLOVER und M. JAQUIER: „Precise QCD predictions for the production of Higgs + jet final states“. *Phys.Lett.* (2015), Bd. B740: S. 147–150 (siehe S. 11).
12. CULLEN, G., H. van DEURZEN, N. GREINER, G. LUISONI, P. MASTROLIA u. a.: „Next-to-Leading-Order QCD Corrections to Higgs Boson Production Plus Three Jets in Gluon Fusion“. *Phys.Rev.Lett.* (2013), Bd. 111(13): S. 131801 (siehe S. 11).
13. DEL DEBBIO, LUIGI, NATHAN P. HARTLAND und STEFFEN SCHUMANN: „MCgrid: projecting cross section calculations on grids“. *Comput.Phys.Commun.* (2014), Bd. 185: S. 2115–2126 (siehe S. 7).
14. DEURZEN, H. van, N. GREINER, G. LUISONI, P. MASTROLIA, E. MIRABELLA u. a.: „NLO QCD corrections to the production of Higgs plus two jets at the LHC“. *Phys.Lett.* (2013), Bd. B721: S. 74–81 (siehe S. 11).
15. DITTMAIER, S. u. a.: „Handbook of LHC Higgs Cross Sections: 1. Inclusive Observables“. (2011), Bd. (siehe S. 10).
16. DITTMAIER, S., S. DITTMAIER, C. MARIOTTI, G. PASSARINO, R. TANAKA u. a.: „Handbook of LHC Higgs Cross Sections: 2. Differential Distributions“. (2012), Bd. (siehe S. 13).
17. DJOUADI, A., M. SPIRA und P.M. ZERWAS: „Production of Higgs bosons in proton colliders. {QCD} corrections“. *Physics Letters B* (1991), Bd. 264(3–4): S. 440–446 (siehe S. 11).

18. DJOUADI, ABDELHAK: „The Anatomy of electro-weak symmetry breaking. I: The Higgs boson in the standard model“. *Phys.Rept.* (2008), Bd. 457: S. 1–216 (siehe S. 11).
19. FLORIAN, D. de, M. GRAZZINI und Z. KUNSZT: „Higgs production with large transverse momentum in hadronic collisions at next-to-leading order“. *Phys.Rev.Lett.* (1999), Bd. 82: S. 5209–5212 (siehe S. 11).
20. FRIXIONE, STEFANO und BRYAN R. WEBBER: „Matching NLO QCD computations and parton shower simulations“. *JHEP* (2002), Bd. 0206: S. 029 (siehe S. 5).
21. GEORGI, H. M., S. L. GLASHOW, M. E. MACHACEK und D. V. NANOPoulos: „Higgs Bosons from Two-Gluon Annihilation in Proton-Proton Collisions“. *Phys. Rev. Lett.* (11 März 1978), Bd. 40: S. 692–694 (siehe S. 10).
22. GRAUDENZ, D., M. SPIRA und P. M. ZERWAS: „QCD corrections to Higgs-boson production at proton-proton colliders“. *Phys. Rev. Lett.* (10 März 1993), Bd. 70: S. 1372–1375 (siehe S. 11).
23. HARLANDER, ROBERT V. und WILLIAM B. KILGORE: „Next-to-Next-to-Leading Order Higgs Production at Hadron Colliders“. *Phys. Rev. Lett.* (20 Mai 2002), Bd. 88: S. 201801 (siehe S. 11).
24. HEINEMEYER, S u. a.: „Handbook of LHC Higgs Cross Sections: 3. Higgs Properties“. (2013), Bd. Hrsg. von HEINEMEYER, S (siehe S. 13).
25. KLUGE, T., K. RABBERTZ und M. WOBISCH: „FastNLO: Fast pQCD calculations for PDF fits“. (2006), Bd.: S. 483–486 (siehe S. 8).
26. KUNSZT, ZOLTAN und DAVISON E. SOPER: „Calculation of jet cross sections in hadron collisions at order α_s^3 “. *Phys. Rev. D* (1 Juli 1992), Bd. 46: S. 192–221 (siehe S. 3).
27. LAI, HUNG-LIANG, MARCO GUZZI, JOEY HUSTON, ZHAO LI, PAVEL M. NADOLSKY u. a.: „New parton distributions for collider physics“. *Phys.Rev.* (2010), Bd. D82: S. 074024 (siehe S. 19).

28. RAVINDRAN, V., J. SMITH und W.L. VAN NEERVEN: „Next-to-leading order QCD corrections to differential distributions of Higgs boson production in hadron hadron collisions“. *Nucl.Phys.* (2002), Bd. B634: S. 247–290 (siehe S. 11).
29. WOBISCH, M., D. BRITZGER, T. KLUGE, K. RABBERTZ und F. STOBER: „Theory-Data Comparisons for Jet Measurements in Hadron-Induced Processes“ (2011), Bd. (siehe S. 8).

Danksagung

Erklärung nach §13(8) der Prüfungsordnung für den Bachelor-Studiengang Physik und den Master-Studiengang Physik an der Universität Göttingen:

Hiermit erkläre ich, dass ich diese Abschlussarbeit selbstständig verfasst habe, keine anderen als die angegebenen Quellen und Hilfsmittel benutzt habe und alle Stellen, die wörtlich oder sinngemäß aus veröffentlichten Schriften entnommen wurden, als solche kenntlich gemacht habe.

Darüberhinaus erkläre ich, dass diese Abschlussarbeit nicht, auch nicht auszugsweise, im Rahmen einer nichtbestandenen Prüfung an dieser oder einer anderen Hochschule eingereicht wurde.

Göttingen, den 11. Juli 2015

(Timo Janßen)

Liste der noch zu erledigenden Punkte
